

Can Tetrazole-functionalized Ligands Realize the Role-control of Keggin-type POMs in Hybrid Framework?

Supporting Information

Table S1. Selected Bond lengths (Å) and angles (°) for compounds **1-4**.

Compound 1			
Cu(1)-O(2W)	1.928(9)	Cu(2)-O(3W)#1	1.946(8)
Cu(1)-O(1W)	1.927(12)	Cu(2)-N(9)	2.000(11)
Cu(1)-N(1)	1.950(9)	Cu(2)-N(13)	2.061(11)
Cu(1)-N(5)	2.002(10)	Cu(2)-O(3W)	1.944(9)
O(2W)-Cu(1)-O(1W)	88.3(5)	O(3W)#1-Cu(2)-N(9)	89.2(5)
O(2W)-Cu(1)-N(1)	92.3(4)	O(3W)-Cu(2)-N(13)	90.1(4)
O(1W)-Cu(1)-N(1)	170.0(5)	O(3W)#1-Cu(2)-N(13)	175.4(4)
O(2W)-Cu(1)-N(5)	168.2(4)	N(9)-Cu(2)-N(13)	90.9(5)
O(1W)-Cu(1)-N(5)	92.1(4)	O(3W)-Cu(2)-Cu(2)#1	46.8(2)
N(1)-Cu(1)-N(5)	89.3(4)	O(3W)#1-Cu(2)-Cu(2)#1	46.7(3)
O(3W)-Cu(2)-O(3W)#1	89.8(4)	N(9)-Cu(2)-Cu(2)#1	131.9(4)
O(3W)-Cu(2)-N(9)	178.6(4)	N(13)-Cu(2)-Cu(2)#1	134.6(3)
Compound 2			
Cu(1)-N(1)	2.013(11)	Cu(1)-N(2)#3	2.080(12)
Cu(1)-N(5)#4	1.979(12)	Cu(1)-Cl(1)	2.468(2)
N(5)#4-Cu(1)-N(1)	123.3(5)	N(5)#4-Cu(1)-Cl(1)	105.3(4)
N(5)#4-Cu(1)-N(2)#3	114.1(5)	N(1)-Cu(1)-Cl(1)	100.7(4)
N(1)-Cu(1)-N(2) #3	112.3(5)	N(2)#3-Cu(1)-Cl(1)	95.7(4)
Compound 3			
Ag(1)-N(10)	2.215(9)	Ag(2)-N(9)	2.468(9)
Ag(1)-N(1)	2.251(9)	Ag(3)-N(13)	2.216(8)
Ag(1)-N(5)	2.434(10)	Ag(3)-N(19)#1	2.257(9)
Ag(2)-N(21)	2.206(8)	Ag(3)-N(22)	2.297(9)
Ag(2)-N(6)	2.236(10)		
N(10)-Ag(1)-N(1)	160.8(3)	N(6)-Ag(2)-N(9)	122.6(3)
N(10)-Ag(1)-N(5)	120.1(3)	N(13)-Ag(3)-N(19)#1	126.9(3)
N(1)-Ag(1)-N(5)	77.7(3)	N(13)-Ag(3)-N(22)	110.0(3)
N(21)-Ag(2)-N(6)	138.4(3)	N(19)#1-Ag(3)-N(22)	120.8(3)
N(21)-Ag(2)-N(9)	98.8(3)		
Compound 4			
Ag(1)-N(1)	2.278(10)	Ag(2)-N(15)#3	2.447(10)
Ag(1)-N(9)	2.351(10)	Ag(3)-O(2W)	2.47(3)
Ag(1)-N(14)#1	2.356(10)	Ag(3)-N(2)#4	2.336(13)
Ag(2)-N(6)	2.214(9)	Ag(3)-O(1W)	2.458(19)
Ag(2)-N(10)#2	2.237(10)	Ag(3)-N(7)	2.472(10)
N(1)-Ag(1)-N(9)	130.9(3)	O(2W)-Ag(3)-N(2)#4	138.3(11)
N(1)-Ag(1)-N(14)#1	122.7(3)	O(2W)-Ag(3)-O(1W)	87.0(9)

N(9)-Ag(1)-N(14)#1	103.8(3)	N(2)#4-Ag(3)-O(1W)	85.3(5)
N(6)-Ag(2)-N(10)#2	159.7(4)	O(2W)-Ag(3)-N(7)	96.7(9)
N(6)-Ag(2)-N(15)#3	103.6(3)	N(2)#4-Ag(3)-N(7)	116.7(4)
N(10)#2-Ag(2)-N(15)#3	93.2(4)	O(1W)-Ag(3)-N(7)	136.3(5)

Symmetry code: for **1**: #1 -x+2, y, -z+1/2; for **2**: #3 +Y, 1-X, +Z; #4 -X, 1-Y,+Z; for **3**: #1 -x+3/2, y-1/2, z; for **4**: #1 1-X, 1/2+Y, 3/2-Z; #2 1+X, 3/2-Y, 1/2+Z; #3 2-X, 1-Y, 2-Z; #5 2-X, 2-Y, 2-Z.

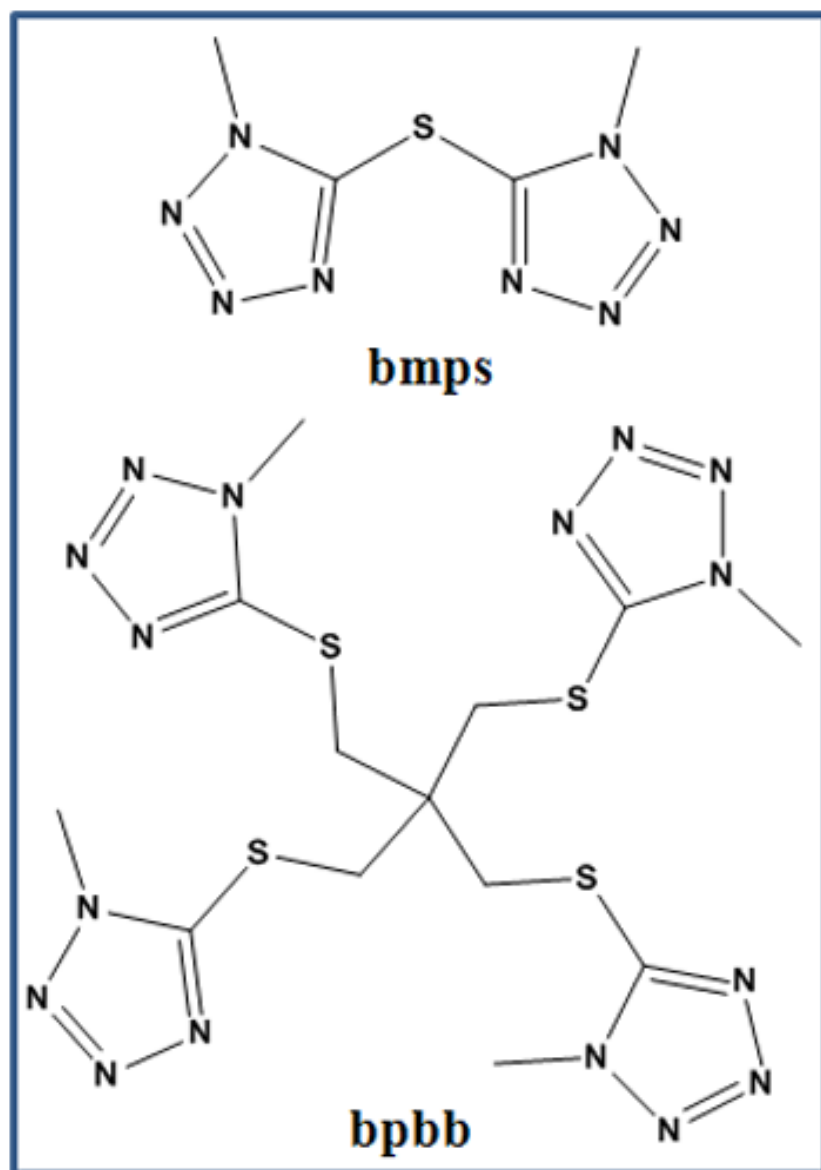


Chart S1. Tetrazole-functionalized flexible ligands bmps and bpbb used in this paper.

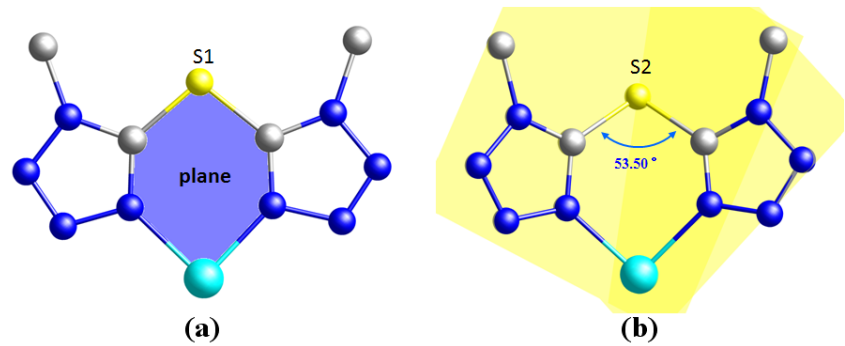


Figure S1. Bidentate metal-chelate coordination modes of bmps ligands with different dihedral angles of bmps^1 (a) and bmps^2 (b) in **1**.

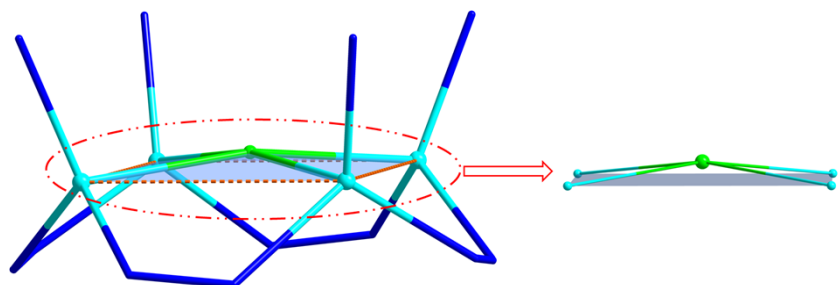


Figure S2. Trigonal-pyramidal geometry of $[\text{Cu}_4(\mu_4\text{-Cl})]$ core in **2**. Such geometry could provide more opportunities for the internal Cu ions to coordinate with external other donor atoms rather.

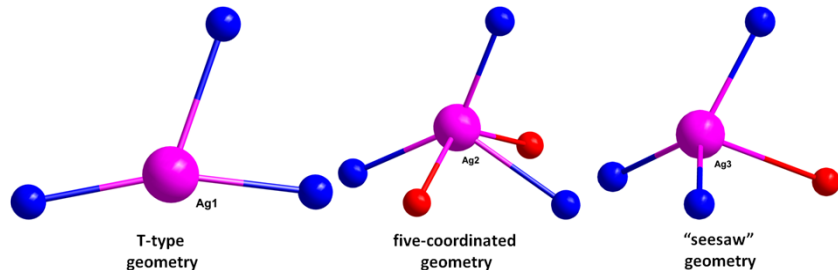


Figure S3. Three kinds of coordination geometries of independent Ag^+ ions in **3**.

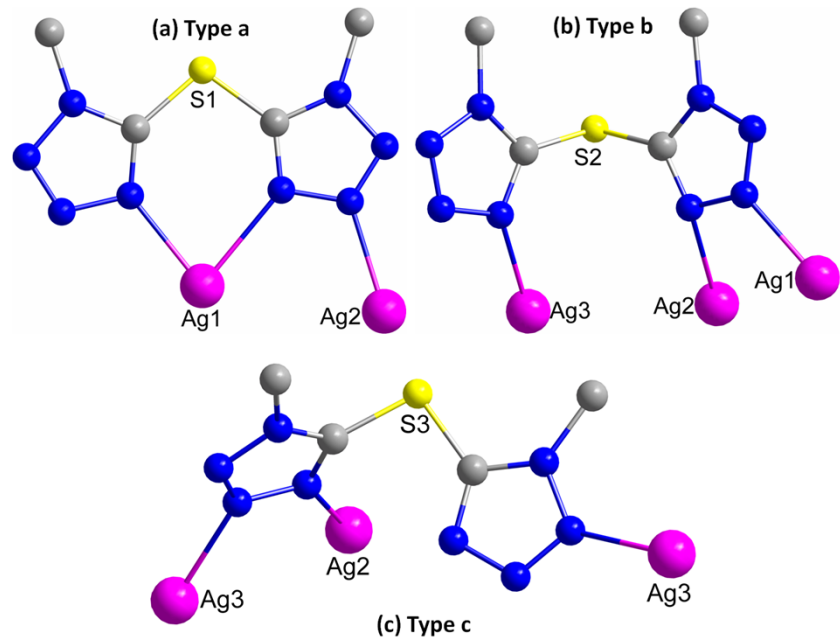


Figure S4. Diverse coordination modes of bmps ligands in **3**.

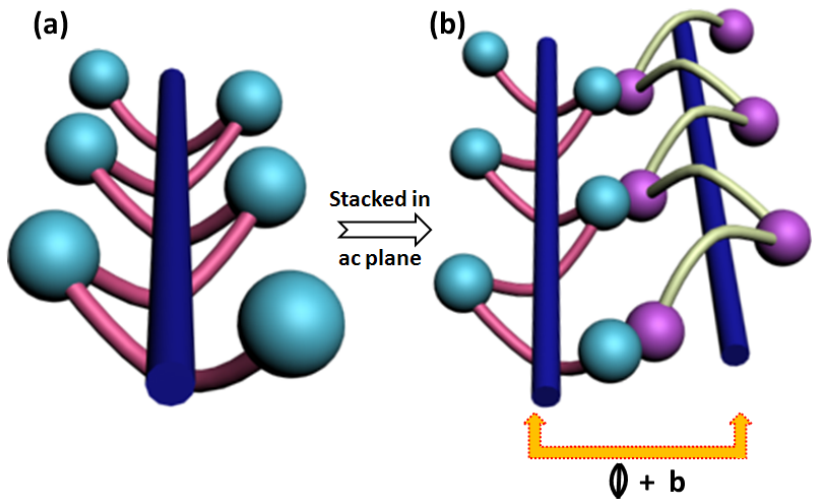


Figure S5. Through two symmetry operators (2-fold rotation and \mathbf{b} translation), the adjacent 1D chains are arranged in an antiparallel manner and slightly shift along \mathbf{b} axis to decrease the steric hindrance.

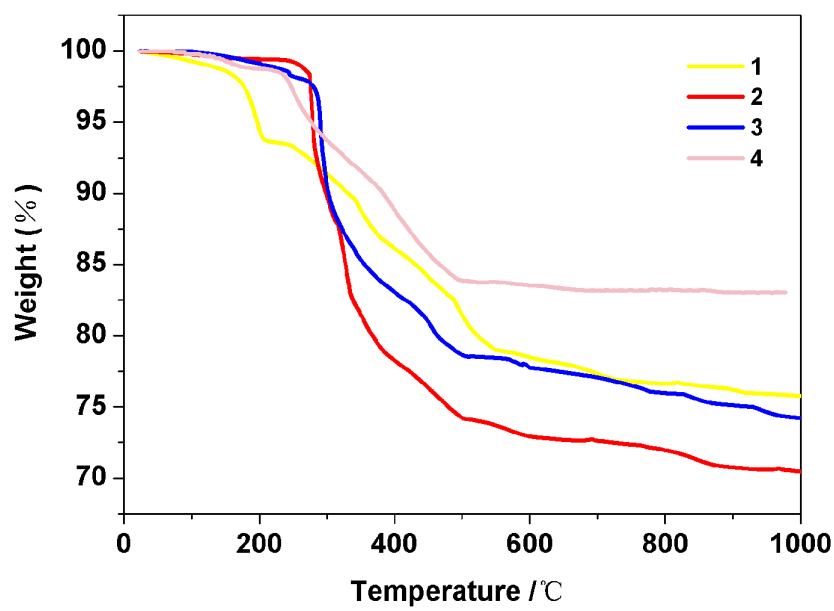


Figure S6. TG curves of compounds 1-4.

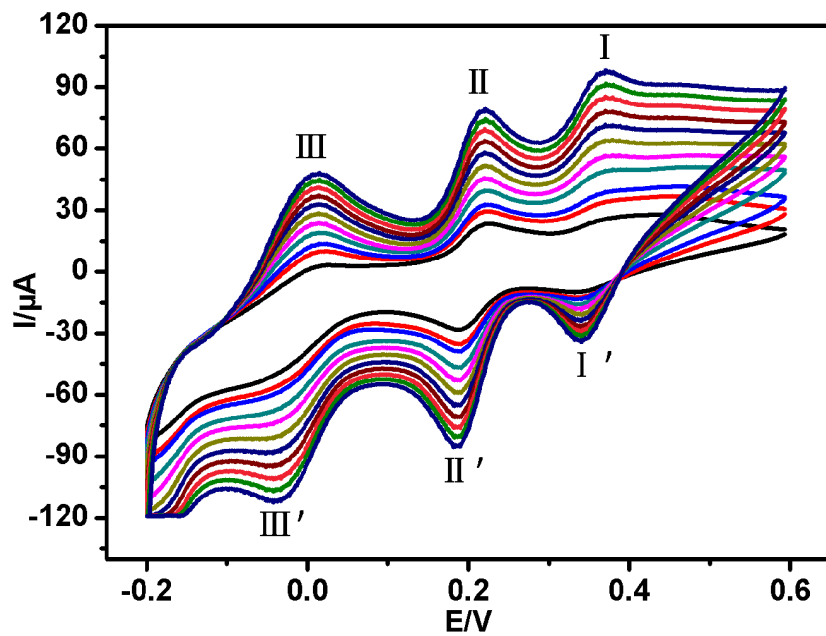


Figure S7. Cyclic voltammograms of the 1-CPE in 1M H_2SO_4 aqueous solution at different scan rates (from inner to outer: 50, 80, 100, 150, 200, 250, 300, 350, 400, 450, 500 mVs^{-1}).

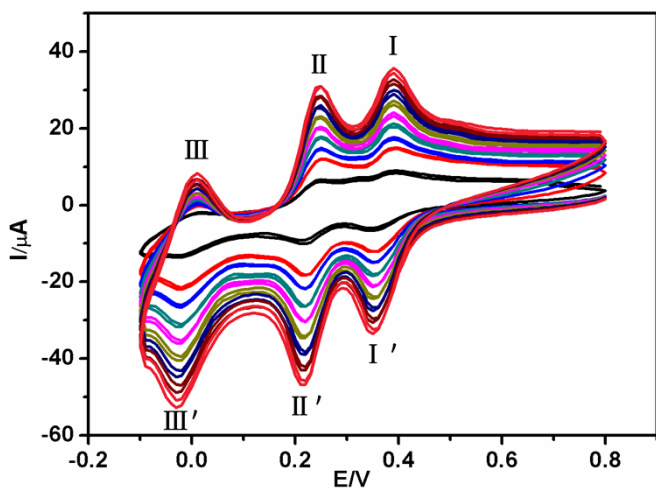


Figure S8. Cyclic voltammograms of the **2**-CPE in 1M H_2SO_4 aqueous solution at different scan rates (from inner to outer: 50, 100, 150, 200, 250, 300, 350, 400, 450 mVs^{-1}).

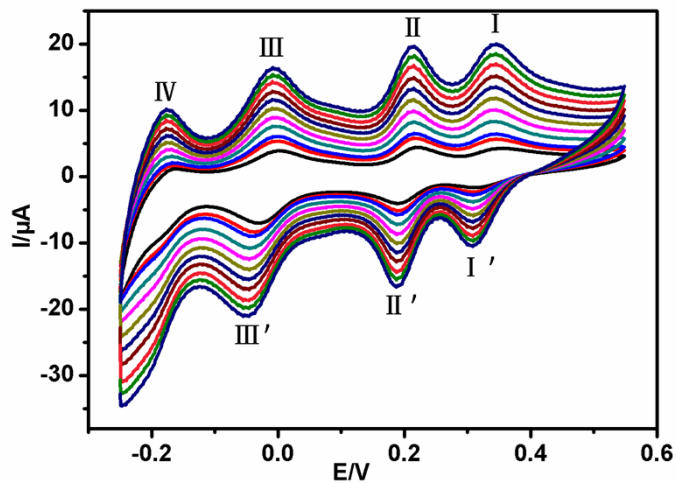


Figure S9. Cyclic voltammograms of the **4**-CPE in 1M H_2SO_4 aqueous solution at different scan rates (from inner to outer: 50, 80, 100, 150, 200, 250, 300, 350, 400, 450, 500 mVs^{-1}).

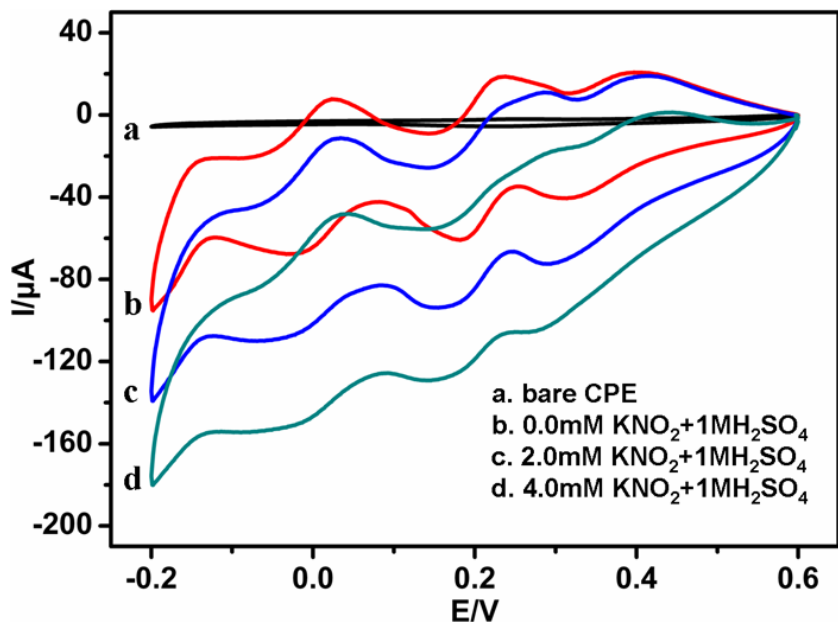


Figure S10. Cyclic voltammograms of **3**-CPE in a 1M H₂SO₄ solution containing 0.0-4.0 mM KNO₂ and a bare CPE in a 2 mM KNO₂ + 1M H₂SO₄ solution. Potentials vs SCE. Scan rate: 120 mV/s.

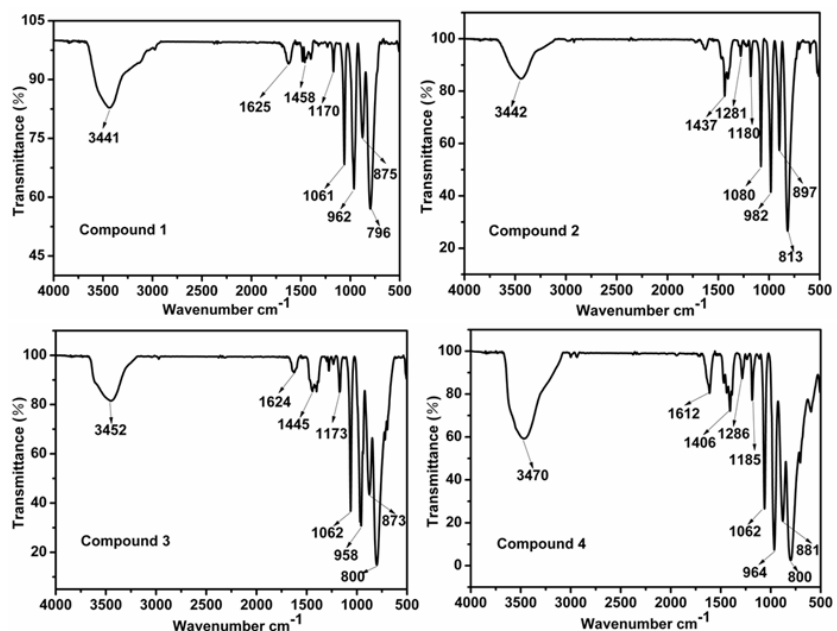


Figure S11. IR spectra of compounds **1-4**. Characteristic bands at 796, 875, 962, and 1061 cm⁻¹ for **1**, 813, 897, 982 and 1080 cm⁻¹ for **2**, 800, 873, 958 and 1062 cm⁻¹ for **3**, 800, 881, 964 and 1062 cm⁻¹ for **4** are attributed to $\nu(\text{M}-\text{O}-\text{M})$, $\nu(\text{M}=\text{O})$, and $\nu(\text{P}-\text{O})$, ($\text{M} = \text{W}, \text{Mo}$), respectively. Bands in the region of 1170-1630 cm⁻¹ are assigned to the vibrations of the flexible ligands, respectively.

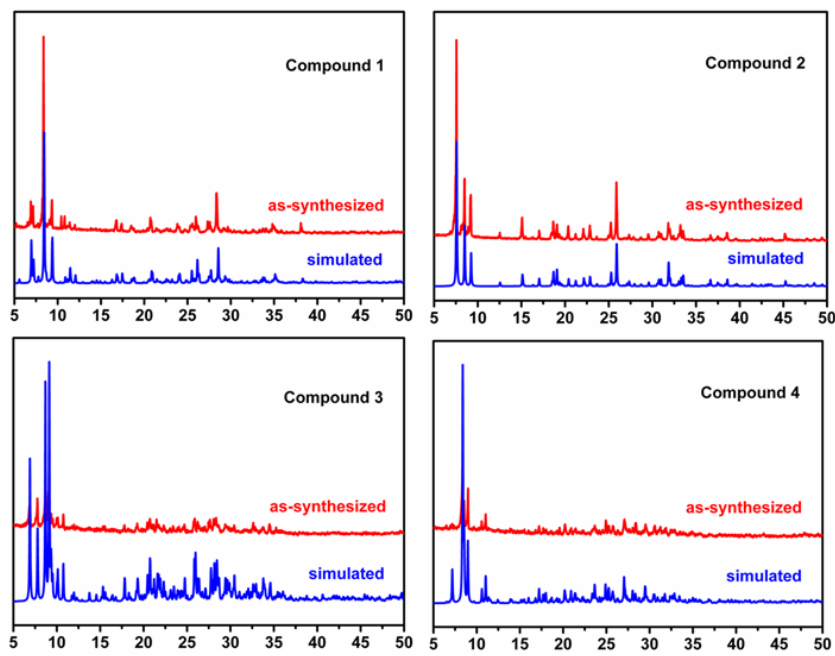


Figure S12. Experimental and simulated XRPD patterns of compounds 1-4. The diffraction peaks of both simulated and experimental patterns match in the key positions, indicating the phase purities of the four compounds.